

not strong. From the observed pattern of yields it was concluded that the much smaller quantum yields for radicals with an RCO group on the ring was explained by differences in the detailed nature of the electronic state of the anion radical rather than any decrease in the energy available to the departing electron.

*Acknowledgment.* The research described herein was supported by the Office of Basic Energy Sciences of the Department of Energy. This is Document No. NDRL-3168 from the Notre Dame Radiation Laboratory. The authors also thank Dr. P. V. Kamat for his help with the electrochemical measurements.

## Growth Mechanisms of Silver Halide Clusters from the Molecule to the Colloidal Particle

David Hayes, Klaus H. Schmidt, and Dan Meisel\*

Chemistry Division, Argonne National Laboratory, Argonne, Illinois 60439 (Received: September 2, 1988; In Final Form: March 22, 1989)

Studies of growing silver halide clusters, from the molecular level to colloidal-size particles, have been undertaken and correlations between particle size and physical properties have been investigated. The production of halide ions by dissociative electron attachment following pulse radiolysis of methylene halide solutions was utilized to instantaneously produce homogeneous, supersaturated solutions of halide and silver ions. The growth of silver halide particles in these solutions has been examined by conductance, absorption spectroscopy, and light scattering measurements. Conductivity measurements show that the initial reaction between the ions occurs at a diffusion-controlled rate and allow determination of the stability constants of molecular silver halide species. In solutions containing excess silver ions, particle growth of silver iodide and silver bromide occurs via a diffusion-controlled aggregation mechanism during the first seconds. The growth rate is reduced significantly, due to electrostatic repulsion between particles, when the concentration of halide ions is almost equal to or greater than the stoichiometric concentration of silver ions. The absorbance of silver iodide suspensions produced in this manner has also been measured. The initial absorbance, due to AgI molecules, occurs at wavelengths of 280 nm and below. The lowest energy exciton band appears  $\sim 50 \mu\text{s}$  after initiation of the reaction. This band initially peaks at around 320 nm and shifts toward 425 nm (the wavelength of exciton absorption in "bulk" silver iodide). The surface potential at the interface evolves at about the same rate as the bulk properties of the material. For the mostly dissociated AgCl molecules growth by addition of ions to a small number of particles of critical size was observed.

### Introduction

Much attention has been paid in recent years to the photo-physical and electrochemical properties of particles of colloidal dimensions with regard to their utility in the promotion and catalysis of reactions.<sup>1</sup> In particular, the changes in band-gap energies and spectroscopic and electrical properties of very small particles have been examined in detail for several semiconductors as the particle radius is reduced.<sup>1,2</sup> For silver halides Berry<sup>3</sup> originally noted alterations in the absorption spectrum of silver halide sols and attributed this effect to the presence of very small particles. More recently Tanaka et al.<sup>4</sup> have undertaken extensive studies on the absorption of various silver halide and mixed silver halide species on the millisecond or slower time scales, utilizing a multichannel spectrophotometer and rapid mixing chamber. Their results showed that dramatic changes in the absorption properties of these species occurs during particle growth. Some of these variations were attributed to the presence of complex ionic species in solution or to changing crystalline structures of the silver halide producing different absorption properties. However, additional variations in the spectra were due to small particle sizes which led to an increase in the energy of threshold absorption due to confinement of the electron-hole pairs in the crystallites. Brus and co-workers<sup>5a</sup> have examined this effect theoretically and have

shown that their model for the shifts in band-gap energies was consistent with the variations observed by Tanaka et al.

The importance of silver halides in photographic processes has led to extensive investigations of their properties and intense interest in the mechanisms of their growth.<sup>6</sup> Težak and co-workers<sup>7</sup> examined the precipitation conditions for formation of uniform, finely dispersed AgX species using classical methods. Meehan et al.<sup>8</sup> performed several studies utilizing both conductivity and light scattering measurements to investigate the formation of colloidal AgBr in solution. Their results indicated that the reaction of the ionic species was completed during the mixing process and that aggregation was the dominant growth mechanism during the early stages. In a different approach, Jaycock and Parfitt used in situ silver iodide generation from ethyl iodide on a slow time scale,<sup>9a</sup> eliminating complications due to mixing effects while Klein et al. similarly examined the growth of silver chloride from allyl chloride.<sup>9b</sup>

It is now commonly believed that the growth process of ionic, sparingly soluble salts is a combination of four stages: formation of molecules and complexes, formation and growth of nuclei, aggregation, and ripening. In spite of the impressive volume of data, little is known about the early stages of the growth processes. Testimonial to this lack of reliable information is the recent confusion surrounding the effect of  $\text{Ag}^+$  on the oscillatory Belousov-Zhabotinskii reaction.<sup>10</sup> In this context values as low as

(1) (a) Brus, L. *J. Phys. Chem.* **1986**, *90*, 2555 and references therein. (b) Henglein, A. *Top. Curr. Chem.* **1988**, *143*, 114 and references therein.

(2) (a) Ėfros, A. L.; Ėfros, A. L. *Sov. Phys. Semicond.* **1982**, *16*, 775. (b) Ekimov, A. I.; Onushchenko, A. A. *Sov. Phys. Semicond.* **1982**, *16*, 775. (c) Nedeljković, J. M.; Nenadović, M. T.; Mičić, O. I.; Nozik, A. *J. Phys. Chem.* **1986**, *90*, 12. (d) Lianos, P.; Thomas, J. K. *Chem. Phys. Lett.* **1986**, *125*, 299. (e) Watzke, H. J.; Fendler, J. H. *J. Phys. Chem.* **1987**, *91*, 854. (f) Wang, Y.; Suna, A.; Mahler, W.; Kasowski, R. *J. Chem. Phys.* **1987**, *87*, 7315.

(3) Berry, C. R. *Phys. Rev.* **1967**, *161*, 848. Berry, C. R. *Phys. Rev.* **1967**, *153*, 989.

(4) (a) Tanaka, T.; Matsubara, T.; Saeki, N.; Hada, H. *Photogr. Sci. Eng.* **1976**, *20*, 213. (b) Tanaka, T.; Saijo, H.; Matsubara, T. *J. Photogr. Sci.* **1979**, *27*, 60. (c) Tanaka, T.; Matsubara, T. *Photogr. Sci. Eng.* **1981**, *25*, 1. (d) Saijo, H.; Iwasaki, M.; Tanaka, T.; Matsubara, T. *Photogr. Sci. Eng.* **1982**, *26*, 92. (e) Tanaka, T.; Iwasaki, M. *J. Imaging Sci.* **1985**, *29*, 86.

(5) (a) Rossetti, R.; Hull, R.; Gibson, J. M.; Brus, L. E. *J. Chem. Phys.* **1985**, *83*, 1406. (b) Brus, L. E. *J. Chem. Phys.* **1984**, *80*, 4403.

(6) *The Theory of the Photographic Process*; James, T. H., Ed.; 3rd ed.; Macmillan: New York, 1966.

(7) Težak, B. *Discuss. Faraday Soc.* **1966**, *42*, 175 and references therein.

(8) (a) Meehan, E. J.; Beattie, W. H. *J. Phys. Chem.* **1961**, *65*, 1522. (b) Meehan, E. J.; Chiu, G. J. *J. Phys. Chem.* **1966**, *70*, 1384. (c) Meehan, E. J.; Miller, J. K. *J. Phys. Chem.* **1968**, *72*, 2168.

(9) (a) Jaycock, M. J.; Parfitt, G. D. *Trans. Faraday Soc.* **1961**, *57*, 791. (b) Klein, D. H.; Gordon, L.; Walnut, T. H. *Talanta* **1959**, *3*, 177.

(10) (a) Kshirsagar, G.; Field, R. J.; Györgyi, L. *J. Phys. Chem.* **1988**, *92*, 2472. (b) Noszticzius, Z.; McCormick, W. D. *J. Phys. Chem.* **1988**, *92*, 374.

$10^4 \text{ M}^{-1} \text{ s}^{-1}$  for the rate constant of AgBr formation were estimated.<sup>11</sup> The results presented here show that for all the halides the rate of formation of the AgX molecules from the corresponding ions is very close to the diffusion-control limit.

This study explores the growth kinetics of colloidal silver halide particles and the correlation between the size of the growing particles and their spectroscopic properties, starting at the single molecules and extending to crystallites of bulk properties. Conductivity, light scattering, and absorption measurements are used to enable the whole growth process to be examined. A pulse radiolysis technique is utilized to initiate the production of the silver halide species. Dissociative electron attachment to methylene halides releases halide ions which, in the presence of silver ions, leads to the production of the silver halide salt. The chief advantage of this approach is the essentially instantaneous production of a homogeneous, supersaturated solution of silver and halide ions which allows measurements of the spectroscopic and conductance changes during the whole growth process from the microsecond time region on. An early report of Schiller and Ebert has demonstrated the utility of the pulse radiolysis technique to the initiation of growth of silver chloride.<sup>12a</sup> Preliminary results of such investigations from our laboratory were reported in a previous communication.<sup>12b</sup> In the following, those results are extended to several silver halides under various supersaturation conditions. The production of halide ions via the radiolysis of methylene halides is first briefly discussed. The reaction of the halide ions so produced with silver ions is then examined, and the mechanisms of growth are quantitatively analyzed. Finally, correlations between the spectroscopic properties and particle size are discussed.

### Experimental Section

The pulse radiolysis apparatus with its conductivity and spectrophotometric detection systems has been previously described.<sup>13</sup> Both the streak camera and photomultiplier systems were used in the present study. For short times (up to 1 ms), the photomultiplier was used to record spectra point by point. For longer times spectra were collected as "snapshots", as previously described,<sup>12b</sup> in order to minimize exposure to the analyzing light beam. Pulses of 4-ns to 3- $\mu\text{s}$  width were used to produce  $1 \times 10^{-6}$  to  $5 \times 10^{-4} \text{ M}$  hydrated electrons per pulse.

Unless otherwise stated, all solutions used in this study contained  $10^{-4} \text{ M HClO}_4$ ,  $0.5 \text{ M tert-butyl alcohol}$  to scavenge OH radicals, and were Ar saturated. Silver ions were added as the sulfate salt in the concentration range of  $(0.5\text{--}2.0) \times 10^{-4} \text{ M Ag}^+$ . Solutions were prepared by dissolving the methylene halide in Ar-saturated tert-butyl alcohol which was then mixed under argon with solutions containing the other components. The solutions were mixed immediately before the irradiation in order to minimize hydrolysis of the parent methylene halide molecule or its thermal reaction with the silver ions. Concentrations of methylene halides in the solutions for irradiation were confirmed spectrophotometrically. For most of the experiments in which silver halide particles were generated, concentrations of the methylene halides were  $2.0 \times 10^{-3}$ ,  $1.0 \times 10^{-2}$ , and  $0.1 \text{ M}$  for the iodide, bromide and chloride, respectively.

Transmission electron microscopy and in situ elemental analysis by energy-dispersive X-ray spectroscopy (EDS) of the particles deposited on carbon-coated copper grids were carried out on a Philips EM 420 instrument. Irradiated solutions were diluted with 0.1% poly(vinyl alcohol) (to slow down any further growth) and deposited on the grids within minutes after the irradiation. Examination under the microscope revealed particles whose size distribution was dependent on the conditions of creation of the silver halide. Typically, for AgBr, particles of spherical or cubic

shapes of  $60 \pm 10 \text{ \AA}$  were observed. For AgI, particles of both triangular and spherical shapes were usually observed with a rather broad size distribution. Electron diffraction patterns corresponding to cubic AgBr ( $a = 5.76 \text{ \AA}$ ) and wurzite structure of  $\beta\text{-AgI}$  ( $a = 4.59 \text{ \AA}$ ,  $c = 7.51 \text{ \AA}$ ) were obtained. EDS analysis showed only the corresponding silver and halide lines. For AgCl, we expect only the cubic structure.

For light scattering measurements a 5-mW Hughes (Model 3225H-PC) He-Ne laser was used. The scattered light was measured at  $90^\circ$  and perpendicular to the plane of polarization to the incident light. Since the radii of the particles of interest in this study are much smaller than the excitation wavelength ( $632.8 \text{ nm}$ ), all measurements were in the Rayleigh regime and no Mie corrections are necessary.<sup>14</sup> Also, the particles could be treated as transparent at the excitation wavelength. Size calibration was performed according to a method similar to that of Hsu et al.<sup>15a</sup> Briefly, the turbidity,  $\tau$ , of several Ludox solutions at various concentrations (dilute enough to avoid interference from multiple scattering) was measured on a Varian 2300 spectrophotometer at the wavelength of the laser. The Rayleigh parameter,  $R_{90}$ , for the above described configuration is defined as<sup>15b</sup>

$$R_{90} = 9\pi^2 N v^2 \eta^2 / (2\lambda^4) \quad (\text{I})$$

where  $N$  is the concentration of particles,  $v$  is the volume of a particle,  $\lambda$  is the wavelength of incident light in the solvent used, and  $\eta = (n^2 - 1)/(n^2 + 2)$ , where  $n = n_p/n_0$  is the refractive index of the particle material relative to that of the solvent.  $R_{90}$  for the Ludox solutions were determined from the turbidity measurements according to eq II.<sup>15b</sup> The intensity of scattered light from these

$$R_{90} = 3\tau / (16\pi) \quad (\text{II})$$

Ludox solutions was then measured, by using the same geometry as that used for the irradiated solutions, to provide a calibration factor for conversion of the scattered light signals to  $R_{90}$  values. The following values were used in eq I:  $n_0 = 1.3318$ ;  $n_p = 2.071$ ,  $2.253$ , and  $2.22$  for AgCl, AgBr, and AgI, respectively.<sup>16</sup> The total volume of the scattering particles ( $Nv$  in eq I) was determined from the known concentration of halide ions produced by the irradiation or silver ions, whichever was the limiting concentration, and the molecular weights,  $M_w$ , and densities,  $\rho$ , of the corresponding bulk silver halide material ( $\rho = 5.56$ ,  $6.47$ , and  $6.01 \text{ g/cm}^3$  for AgCl, AgBr, and AgI, respectively)<sup>16</sup>, according to eq III. By use of eq I and III,  $N$  and  $v$  can be evaluated. For a

$$Nv = M_w[\text{AgX}] \times 10^{-3} / \rho \quad (\text{III})$$

distribution of particle sizes, this method yields the volume-weighted average volume of a particle, i.e.,  $v = (\sum N v_i^2) / (\sum N v_i)$ . It is important to realize that the underlying assumption in using eq I and III is that the total scattering volume,  $Nv$ , is constant during the time of observation. If not all of the AgX material has been converted to particles of sizes at which the bulk density applies, this assumption will be wrong. Our spectrophotometric and conductivity results indicate that in the time regimes where light scattering measurements are feasible for AgBr and AgI the concentration of molecular species remaining in the solution is negligible for most of the results reported here. This, however, is not the case for AgCl at low concentrations, as will be elaborated separately below.

### Results and Discussion

*A. Release of Halide Ions from Methylene Halides.* Before proceeding to the silver halide systems, the radiation chemistry of the methylene halides, which were used to produce the halide ions, has to be understood. This section describes the radiation

(11) (a) Ruoff, P. *Chem. Phys. Lett.* **1982**, *92*, 239. (b) Ruoff, P.; Schwitters, B. *J. Phys. Chem.* **1984**, *88*, 6424; *Ibid.* **1986**, *90*, 2497.

(12) (a) Schiller, R.; Ebert, M. *Int. J. Radiat. Phys. Chem.* **1969**, *1*, 111.

(b) Schmidt, K. H.; Patel, R.; Meisel, D. *J. Am. Chem. Soc.* **1988**, *110*, 4882.

(13) (a) Schmidt, K. H.; Gordon, S. *Rev. Sci. Instrum.* **1979**, *50*, 1656. (b) Schmidt, K. H.; Gordon, S.; Thompson, M.; Sullivan, J. C.; Mulac, W. A. *Radiat. Phys. Chem.* **1983**, *21*, 321.

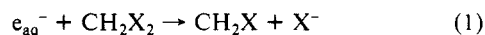
(14) (a) Berry, C. R. *J. Opt. Soc. Am.* **1962**, *52*, 888. (b) Meehan, E. J.; Beattie, W. H. *J. Phys. Chem.* **1960**, *64*, 1006.

(15) (a) Hsu, W. P.; Patel, R. C.; Matijević, E. *Appl. Spectrosc.* **1987**, *41*, 402. (b) Kerker, M. *The Scattering of Light and Other Electromagnetic Radiation*; Academic Press: New York, 1969; pp 31-39.

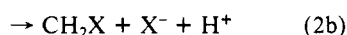
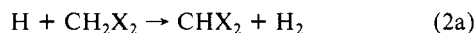
(16) *Landolt-Börnstein, New Series*; Springer Verlag: Berlin, Heidelberg, New York, 1982; Vol. 17b, pp 297-301.

chemistry of these compounds, and the next one explores the possible effects of reactions of  $\text{Ag}^+$  with the radicals involved. The relevance of these two sections to the main theme is limited to the conclusion that interference from the radiation chemistry of the system with the growth of silver halides is minimal.

A large number of publications describe the reactions of solvated electrons or hydrogen atoms with alkyl halides.<sup>17</sup> The reaction of  $e_{\text{aq}}^-$  with alkyl halides is commonly believed to proceed through

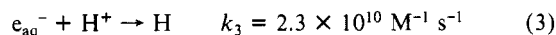


dissociative addition, releasing the halide ion and producing the corresponding alkyl radical. The reaction of hydrogen atoms can

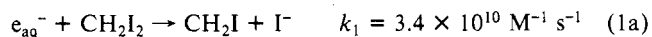


proceed either through hydrogen abstraction or through halide elimination. The latter (reaction 2b) is believed to be the main pathway for the iodides, and the former is the major route for the chlorides. Hydrolysis of the resultant alkyl halide radical, when more than one halide is present in the parent molecule, has been observed for combinations of fluoro- and chloromethyl radicals<sup>18</sup> but is very slow for other halide-substituted methyl radicals.<sup>19</sup> Under the present experimental conditions of relatively high radical concentrations, radical-radical recombination dominates. Several halomethyl radicals have been shown to be strong oxidants.<sup>20</sup>

Of primary interest in the present study are the rates of reactions 1 and 2 and the relative contributions of reactions 2a and 2b. Since the optical spectra provide only marginal information on the identity of the radicals, efforts were focused on the conductivity technique. Figure 1 displays the conductivity changes observed in several solutions with increasing  $\text{CH}_2\text{I}_2$  concentrations at pH 4.0 following a pulse that produces a total of  $[e_{\text{aq}}^-] + [\text{H}] = 4.5 \times 10^{-6}$  M. The fast initial decay of the conductivity signal in Figure 1 is due to the reaction of  $e_{\text{aq}}^-$  with protons. This reaction



competes with reaction 1a, which becomes dominant as the  $\text{CH}_2\text{I}_2$



concentration increases. As can be seen in Figure 1, the conductivity signal recovers as the H atoms, produced in reaction 3 and by direct radiolysis of water, react with  $\text{CH}_2\text{I}_2$ . Both the rate of recovery and the level to which the signal recovers depend on  $\text{CH}_2\text{I}_2$  concentration. For the highest  $\text{CH}_2\text{I}_2$  concentration used ( $1 \times 10^{-3}$  M) the amplitude of the conductivity signal at the end of this recovery process corresponds quantitatively to the expected amplitude assuming  $\kappa = \{\lambda(\text{H}^+) + \lambda(\text{I}^-)\}G(e_{\text{aq}}^- + \text{H})D$ , where  $D$  is the dose in units of  $100 \text{ eV/cm}^2$ ,  $G(e_{\text{aq}}^- + \text{H}) = 3.35$  radicals/100 eV, and  $\lambda(\text{H}^+) = 350 \text{ S cm}^2$  and  $\lambda(\text{I}^-) = 76 \text{ S cm}^2$  are the equivalent conductances of  $\text{H}^+$  and  $\text{I}^-$ , respectively. This leads to the conclusion that protons are indeed released in reaction 2 and that both  $e_{\text{aq}}^-$  and H atoms produce  $\text{I}^-$  ions and methylene iodide radicals on reacting with  $\text{CH}_2\text{I}_2$ ; i.e.,  $k_{(2a)} \ll k_{(2b)}$ . To confirm this conclusion, the signal amplitude was also measured in  $\text{N}_2\text{O}$ -saturated solutions containing  $4 \times 10^{-5}$  M  $\text{CH}_2\text{I}_2$  and 0.5 M *tert*-butyl alcohol, where the only radicals that may react with  $\text{CH}_2\text{I}_2$  are H atoms. The amplitude of the conductivity signal in these experiments corresponds to complete scavenging of H atoms and release of the  $\text{H}^+$  and  $\text{I}^-$  ions. Most probably reaction

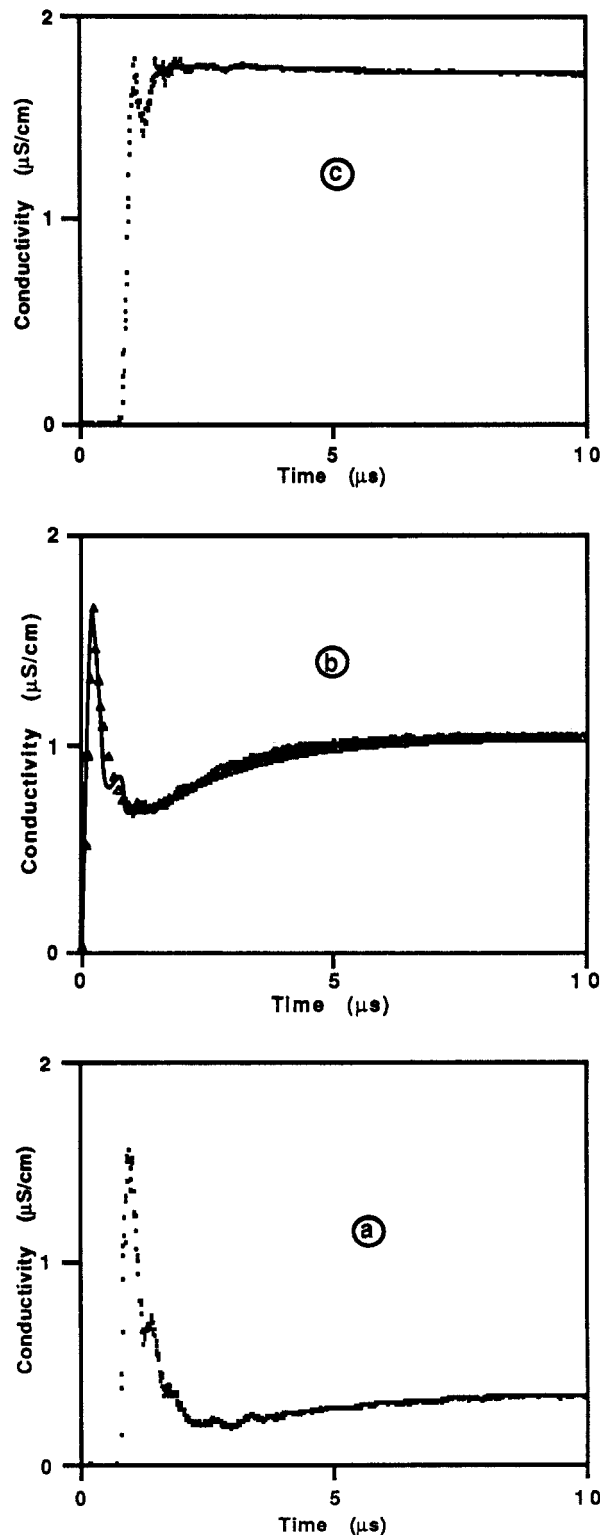
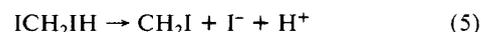


Figure 1. Conductivity signals following pulse irradiation of Ar-saturated solutions of various  $\text{CH}_2\text{I}_2$  concentrations at pH 4 in the presence of 0.5 M *tert*-butyl alcohol.  $[\text{CH}_2\text{I}_2] =$  (a)  $2.2 \times 10^{-5}$  M, (b)  $4.5 \times 10^{-5}$  M, and (c)  $4.5 \times 10^{-4}$  M. Triangles in curve b are simulated results calculated as explained in the text.

2 is not an outer-sphere electron-transfer reaction since large solvent reorganization energies are involved in the  $\text{H}/\text{H}^+$  oxidation and in the release of  $\text{I}^-$ . Rather an addition reaction precedes the iodide release step:



The results indicate that the lifetime of the adduct is too short

(17) Swallow, A. J. *Prog. React. Kinet.* **1978**, *9*, 209 and references therein.

(18) Balkas, T. I.; Fendler, J. H.; Schuler, R. H. *J. Phys. Chem.* **1971**, *75*, 455.

(19) (a) Lesigne, B.; Gilles, L.; Woods, R. *J. Can. J. Chem.* **1974**, *52*, 1135.

(b) Balkas, T. I. *Int. J. Radiat. Phys. Chem.* **1972**, *4*, 199.

(20) (a) Köster, R.; Asmus, K.-D. *Z. Naturforsch.* **1971**, *26B*, 1104. (b) Willson, R. L.; Slater, T. F. In *Fast Processes in Radiation Chemistry and Biology*; Adams, G. E., Fielden, E. M., Michael, B. D., Eds.; Wiley: London, 1975; p 147. (c) Neta, P.; Fessenden, R. W.; Schuler, R. H. *J. Phys. Chem.* **1971**, *75*, 1654.

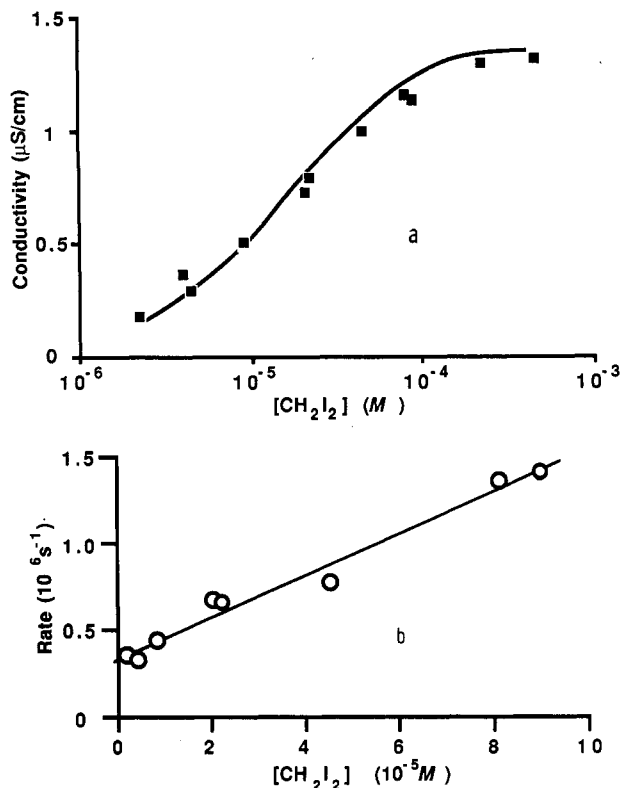
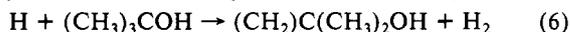


Figure 2. (a) Dependence of the amplitude of the conductivity signal after completion of reaction 2, and (b) dependence of the rate of recovery on  $[\text{CH}_2\text{I}_2]$  at pH 4.0 in the presence of 0.5 M *tert*-butyl alcohol. Solid curve in (a) is the signal calculated by using eq 7; all points are normalized for the same dose (980 rad).

to measure and that reaction 5 follows reaction 4 immediately.

The effect of increasing  $\text{CH}_2\text{I}_2$  concentration on the final amplitude of the conductivity signal and on the rate of its recovery via reaction 2 follows competition kinetics as can be seen in Figure 2. The rate constant obtained for reaction 2 from the slope of Figure 2b is  $k_2 = 1.2 \times 10^{10} \text{ M}^{-1} \text{ s}^{-1}$ . The intercept in this figure is primarily due to the competing reaction of hydrogen atoms with *tert*-butyl alcohol and with impurities in the *tert*-butyl alcohol.<sup>21</sup>



The yield of  $\text{CH}_2\text{I}$  radicals as a function of  $\text{CH}_2\text{I}_2$  concentration can be calculated by

$$G(\text{CH}_2\text{I}) = \alpha G(e_{\text{aq}}^-) + \beta \{G(\text{H}) + (1 - \alpha)G(e_{\text{aq}}^-)\} \quad (7)$$

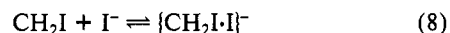
where  $\alpha = k_1[\text{CH}_2\text{I}_2]/\{k_1[\text{CH}_2\text{I}_2] + k_3[\text{H}^+]\}$  and  $\beta = k_2[\text{CH}_2\text{I}_2]/\{k_2[\text{CH}_2\text{I}_2] + k_6[(\text{CH}_3)_3\text{COH}]\}$ . Since  $G(\text{CH}_2\text{I}) = G(\text{H}^+) = G(\text{I}^-)$ , the amplitude of the conductivity signal can be calculated from  $G(e_{\text{aq}}^-)$  and  $G(\text{H})$  yields, the rate constants measured above, the known dose,  $[\text{H}^+]$ ,  $[\text{CH}_2\text{I}_2]$ , and the equivalent conductances quoted above. The fit to the experimental results is shown as the solid curve in Figure 2a. The results of numeric integrations simulating quantitatively the time evolution of the conductivity signals using the rate constants determined above are shown in Figure 1b as triangles. The agreement with the experimental observation is quite good, lending credence to the proposed mechanism. The relevant rate constants are summarized in Table I.

Finally, some observations regarding reactions of the radical on slower time scales may be mentioned. The conductivity signal decays slightly over a period of ca. 50  $\mu\text{s}$  ( $k = 2.2 \times 10^4 \text{ s}^{-1}$ ) and then recovers again on the millisecond time scale. The rate of this process is independent of the concentration of  $\text{CH}_2\text{I}_2$  at the levels where this decay is observable ( $>1 \times 10^{-4} \text{ M}$ ). At lower  $\text{CH}_2\text{I}_2$  concentrations the formation of the radical overlaps this decay process and masks its existence. The amplitude of both

TABLE I: Rate Constants for the Reactions of  $\text{CH}_2\text{X}_2$  and  $\text{Ag}^+$  with  $e_{\text{aq}}^-$  and H Atoms

reaction	rate const, $\text{M}^{-1} \text{ s}^{-1}$	ref
$e_{\text{aq}}^- + \text{CH}_2\text{I}_2$	$3.4 \times 10^{10}$	this work
$e_{\text{aq}}^- + \text{CH}_2\text{Br}_2$	$2 \times 10^{10}$	this work
$e_{\text{aq}}^- + \text{CH}_2\text{Cl}_2$	$6.0 \times 10^9$	37
$e_{\text{aq}}^- + \text{Ag}^+$	$3.7 \times 10^{10}$	37
$\text{H} + \text{CH}_2\text{I}_2$	$1.2 \times 10^{10}$	this work
$\text{H} + \text{CH}_2\text{Br}_2$	$4.1 \times 10^8$	this work
$\text{H} + \text{CH}_2\text{Cl}_2$	$4 \times 10^6$	37
$\text{H} + \text{Ag}^+$	$1.2 \times 10^{10}$	37

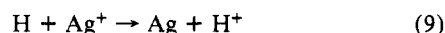
the decayed and recovered signals corresponds quantitatively to the theoretical yield of  $\text{I}^-$  produced in reactions 1 and 2. A possible reaction to account for these observations is formation of a three electron bonded radical anion, akin to the  $\text{I}_2^-$  radical anion:



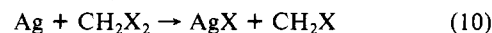
The iodide consumed in reaction 8 is released upon the decay of this radical anion on the slower time scale. As regards the main interest of this report, reaction 8 has no effect on any of the results described below since the reaction of  $\text{Ag}^+$  with  $\text{I}^-$  is much faster than the time scales involved in reaction 8. None of the conductivity changes observed on these slower time scales in the absence of  $\text{Ag}^+$  were observed in its presence. For the other halides these slow reactions were not observed.

Absorption spectra of the  $\text{CH}_2\text{I}$  (or the product of reaction 8) radicals were also briefly studied since they might interfere with the absorptions measured in the presence of  $\text{Ag}^+$ . In the range of 250–400 nm a weak broad absorption peaking at 345 nm ( $\epsilon_{\text{max}} \approx 500 \text{ M}^{-1} \text{ cm}^{-1}$ ) could be observed immediately after the pulse. This absorption was also reported in our previous communication.<sup>12b</sup> At wavelengths below 320 nm bleaching of the methylene iodide could be observed. Both effects contribute very little to the total absorption observed at the early stages of the growth process, and corrections for both were applied in the reported spectra of silver iodide.

**B. Competition by Reactions of  $\text{Ag}^+$  with Radicals.** Examination of the rate constants given in Table I and the concentrations of the various components of the solutions reveals that among the primary radicals only H atoms might react with  $\text{Ag}^+$  in the systems used. Reaction 9 could be quantitatively significant in the case



of the chloride, although even in this case competition by reaction 6 limits its interference. At any rate, formation of silver atoms has little effect on the results described below since they very efficiently react with the alkyl halide to form the corresponding silver halide (reaction 10). Similar reactions with chloroform



and bromoform were previously observed.<sup>22</sup> For  $\text{CH}_2\text{I}_2$  we determined  $k_{10} = 8 \times 10^9 \text{ M}^{-1} \text{ s}^{-1}$ . With such high rate constants any formation of silver atoms will rapidly lead to the production of silver halide at the  $\text{CH}_2\text{X}_2$  concentrations used. Interference from silver atoms in the systems described below is thus negligible.

The possibility of a reaction between silver ions and the secondary radicals ( $\text{CH}_2(\text{CH}_3)_2\text{COH}$  and  $\text{CH}_2\text{X}$ ) should also be considered. Such reactions can occur only at times shorter than 0.1 ms, since this is the longest lifetime of these radicals under the relevant experimental conditions. The  $\beta$ -hydroxy radical from *tert*-butyl alcohol was shown to be unreactive towards silver ions;<sup>22</sup> for the  $\text{CH}_2\text{X}$  radicals we find no evidence of any reaction and the weak absorption due to  $\text{CH}_2\text{I}$  radicals decays at similar rates in the absence or presence of  $\text{Ag}^+$ .

To summarize this and the previous section, release of the halides by the dissociative electron transfer to the alkyl halides is the dominant reaction. Known amounts of halides can therefore be released at predetermined concentrations, and contributions from other species is not a serious problem.

(21) Gordon, S.; Schmidt, K. H.; Hart, E. J. *J. Phys. Chem.* 1977, 81, 104.

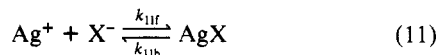
(22) Tausch-Tremml, R.; Henglein, A.; Lilie, J. *Ber. Bunsen-Ges. Phys. Chem.* 1978, 82, 1335.

**TABLE II: Stability and Rate Constants for the Formation of AgX from Conductivity Measurements**

halide	$K_1^a$ , $M^{-1}$	$k_{1f}$ , $M^{-1} s^{-1}$	$k_b^b$ , $s^{-1}$
AgCl	$2.0 \times 10^3$ ( $2.0 \times 10^3$ )	$2.0 \times 10^{10c}$	$9.1 \times 10^6$
AgBr	$2.9 \times 10^4$ ( $4.8 \times 10^4$ )	$1.3 \times 10^{10}$	$4.6 \times 10^5$
AgI	$(3.8 \times 10^6)$	$8.1 \times 10^9$	$2.1 \times 10^3$

<sup>a</sup> Values in parentheses are from ref 38 under conditions specified therein. <sup>b</sup> Calculated from equilibrium constant and  $k_{1f}$ . <sup>c</sup> Assumed based on results from the other halides.

**C. Rate and Stability Parameters of AgX Molecules.** The rate of formation and the stability constants of the silver halides (reaction 11) were measured by following the conductivity changes



in solutions containing  $Ag^+$ . A typical time profile of the conductivity signal was presented in a previous communication.<sup>12b</sup> For AgI and AgBr the rate constants  $k_{1f}$  could be directly measured from the dependence of the conductivity signal decay rate on  $[Ag^+]$  under pseudo-first-order conditions. For AgCl the equilibrium constant  $K_{11}$  is too small to allow direct measurement of  $k_{1f}$  since concentrations of  $Ag^+$  had to be increased to values where the rate became faster than the time resolution of the equipment used. From the conductivity changes at several  $[Ag^+]$  the equilibrium constant  $K_{11}$  was determined by

$$\frac{1}{\Delta\kappa} = \frac{1}{\Delta\kappa_\infty} \left\{ 1 + \frac{1}{K_{11}[Ag^+]} \right\} \quad (12)$$

where  $\Delta\kappa$  is the conductivity change at the end of reaction 11 and the subscript  $\infty$  indicates sufficient  $Ag^+$  concentration to ensure complete shift of equilibrium 11 to the right. Values of  $k_{1b}$  were then calculated from the forward rate constant and the equilibrium constant. The results of these determinations are compiled in Table II. The stability constants presently obtained agree quite well with those previously obtained by using widely different methods. For AgI, the stability constant is too large to be estimated from our results. The kinetic results give forward rate constants close to the diffusion-controlled limit. Earlier estimates<sup>11</sup> of much smaller rate constants could not be substantiated. It is the differences in rate constants for dissociation of the various silver halide molecules that lead to the wide range of stability constants.

For AgI, no further decrease in the conductivity signals was observed for up to 1 s after completion of reaction 11. For AgBr and AgCl, further decrease in the conductivity of the solutions could be observed when the concentration of silver or halide ions was low enough to ensure that equilibrium 11 was not completely shifted to the right. This decrease in conductivity was observed to occur on a much slower time scale, up to ca. 1 s after the pulse and corresponded within experimental accuracy to complete consumption of the halide concentration produced by the irradiation pulse. The rate of this slow decrease in conductivity increased with increasing initial halide concentration. We attribute this decrease in conductivity to consumption of  $Ag^+$  and  $Br^-$  or  $Cl^-$  ions by the growing  $AgX$  nuclei. Indeed, for the growth of AgCl described in section F, a parallel increase in the light scattering is observed.

**D. Spectral Evolution of AgX Molecules and Small Aggregates.** The absorption spectrum of the solution recorded 6  $\mu s$  after the pulse is shown in Figure 3a. With the kinetic information provided in Table II, this spectrum is attributed to the diatomic AgI molecule since at this time 95% of the iodide ions produced have already reacted with silver ions. The absorption rises monotonically to the lower limit of the spectral range (imposed primarily by the absorption of the parent solution). From the concentration of iodide produced by the pulse one calculates  $\epsilon_{250} = 5.2 \times 10^3 M^{-1} cm^{-1}$  for AgI molecules. Similar experiments with 10 times higher iodide concentration produced by the pulse yield a similar absorption spectrum (Figure 3b). Under the latter conditions, however, the concentration of silver ions limits the AgI

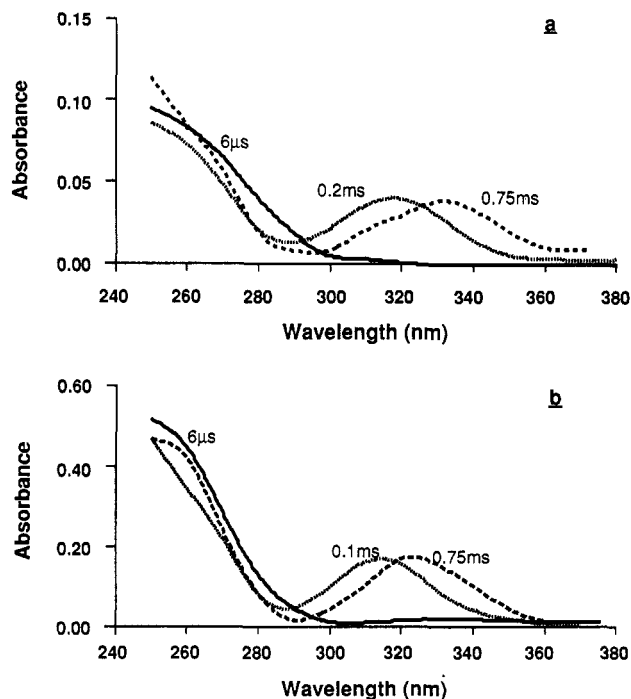
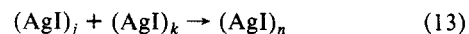


**Figure 3.** Absorption spectra of AgI molecules and small agglomerates at the early stages of formation. Spectra are corrected for bleaching of parent solution and formation of absorbing radicals.  $[Ag^+]_0 = 1 \times 10^{-4} M$ ; (a)  $[I^-]_0 = 2.1 \times 10^{-5} M$ ; (b)  $[I^-]_0 = 2.0 \times 10^{-4} M$ . Spectra recorded at the times indicated after the pulse.  $[CH_2I_2] = 2 \times 10^{-3} M$ ; other conditions as in Figure 1.

concentration and the calculated extinction coefficient is independent of dosimetry. Under these conditions  $\epsilon_{250} = 4.8 \times 10^3 M^{-1} cm^{-1}$  was calculated.

The extent of contributions from other species (complexes, dimers, etc.) to these spectra should now be considered. Since the rate of growth of the absorption is somewhat dependent on the wavelength of observation and a slight red shift is observed at the higher doses, it appears that more than one species contributes to the initial spectra of Figure 3. Yet, the contribution from such species cannot be very large. Computer simulations including the relevant rate constants of Tables I and II and assuming diffusion-controlled rates for agglomeration reactions of the type of reaction 13 were performed for all combinations of



$j$  and  $k$  up to  $n = 10$ .<sup>23</sup> These calculations provide the maximum possible concentrations of  $(AgI)_n$ . The results indicate that at the time the initial spectrum in Figure 3a was recorded no more than 15% of the total  $[AgI]$  could have dimerized. For the higher doses (Figure 3b) the fraction is somewhat higher. When  $[I^-]/[Ag^+] \geq 1$ , small amounts of the complex  $AgI_2^-$  may also contribute, as calculated from the relative stability constants of the molecule and the complex.

As time progresses (10–100  $\mu s$  after the pulse) the band near 250 nm decreases in intensity with concomitant increase in absorption at  $\lambda \geq 300$  nm. At longer times (0.1–1.0 ms) the absorption at the shorter wavelengths slightly increases again while the band at longer wavelengths continues to shift to the red. Spectra corresponding to this time regime are also shown in Figure 3. Kinetic traces showing the decrease and concomitant increase in absorption at shorter and longer wavelengths, respectively, are shown in Figure 4. No isosbestic point was observed, and the spectra therefore cannot be assigned to only two distinct species. Since the absorption spectrum of an aggregate is expected to shift to the red as the particle grows, the wavelength-dependent kinetics

(23) No dissociation was assumed, and the diffusion-controlled rate constant is calculated assuming the same rate constant as  $k_{1f}$ , corrected for the charge effect on reaction 11 using the Debye equation.

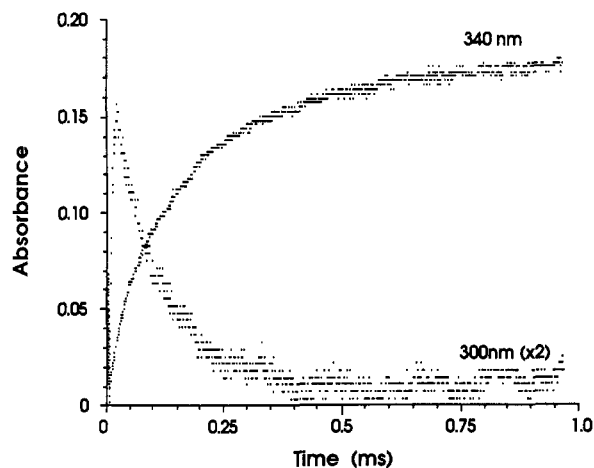


Figure 4. Kinetic traces showing the decrease in absorption at shorter wavelengths and concomitant increase at longer wavelengths. Experimental conditions as in Figure 3b.

reflect the increased contribution of larger aggregates to the absorption spectra at later times. The increase in absorption at shorter wavelengths can be understood assuming that the aggregates have increased to such sizes where the absorption of higher energy bands enters the observation range.

Two further points can be recognized in Figure 3. First, at times longer than  $\sim 100 \mu\text{s}$  the absorbance of the lowest energy band hardly changes as the spectra shift to the red. This indicates that the contribution of each molecule to the absorption at this band is independent of the particle size beyond a certain threshold, which has already been attained at  $\sim 100 \mu\text{s}$  (Figure 3). The oscillator strength from this time on is constant. Second, it can be seen in Figure 3 that the spectra collected under conditions where  $[\text{I}^-]/[\text{Ag}^+] = 1:5$  and  $2:1$  are not identical at any particular time of observation. The broader band obtained with excess of silver ions indicates broader size distributions. Furthermore, this band shifts to longer wavelengths faster in excess  $\text{Ag}^+$  than in excess iodide. It seems, therefore, that in the former case the growth is appreciably faster than in the latter. A similar conclusion is obtained from spectrophotometric and light scattering measurements at longer times.

**E. Growth by Agglomeration.** Growth of the aggregates was further followed to times extending from 1 ms to more than 100 s by using both the light scattering and spectrophotometric techniques. Figure 5 presents successive spectra of growing AgI particles at various times for the two  $[\text{I}^-]/[\text{Ag}^+]$  ratios. The trend previously reported<sup>12b</sup> of a shift in the absorption to lower energies with the growth of the particles is confirmed here. Furthermore, the differences between  $[\text{I}^-]/[\text{Ag}^+] = 1:5$  and  $2:1$  observed at earlier times (Figure 3) extend to much longer times, at least to 1 s. While the spectra for  $[\text{I}^-]/[\text{Ag}^+] = 2:1$  contain a well-defined lowest energy exciton band up to 1 s, those for  $[\text{I}^-]/[\text{Ag}^+] = 1:5$  show this band as a shoulder, typical of the bulk material albeit blue shifted, already at 50 ms. Under the former conditions, the extinction coefficient at the peak of the exciton band is nearly constant up to 1 s and then slightly decreases. In contrast, when  $\text{Ag}^+$  is present in excess, the absorption increases in intensity over the whole spectral range as the spectra shift to the red. This again suggests a broader size distribution under these conditions. The increase in absorption at shorter wavelengths is a result of two effects. First, as discussed by Brus,<sup>5b</sup> the contribution to the absorption intensity from higher energy free electron-hole pairs increases relative to the contribution from the lowest bound exciton state as the size increases. Second, higher exciton bands enter the observable spectral range as the very small aggregates grow to bigger particles. In contrast, when  $\text{I}^-$  is in excess, the size at a given time is smaller and the size distribution is narrower. Most of the absorption intensity is concentrated in the narrow exciton band which dominates the spectra for long times. At times longer than 10 s the distribution broadens and the extinction coefficient drops somewhat at the shorter wavelengths.

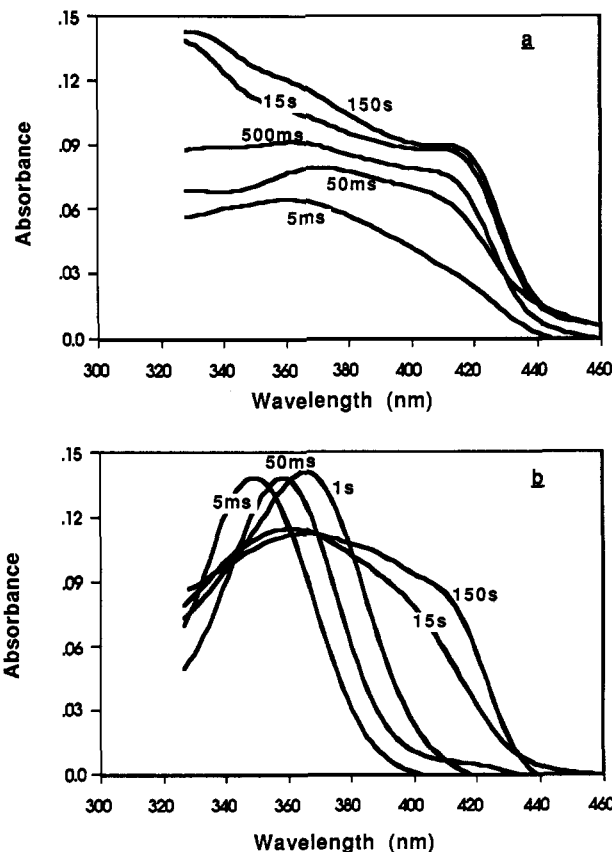


Figure 5. Evolution of absorption spectra of AgI particles at long times; a and b refer to the same experimental conditions as in Figure 3.

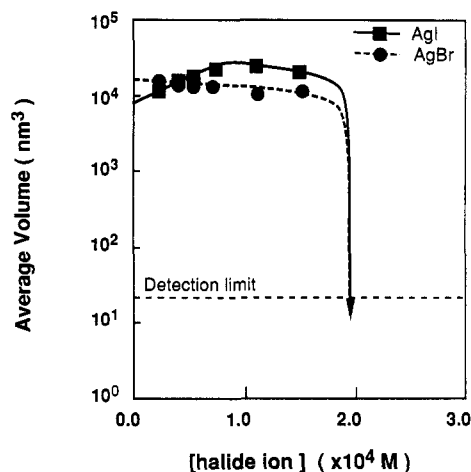
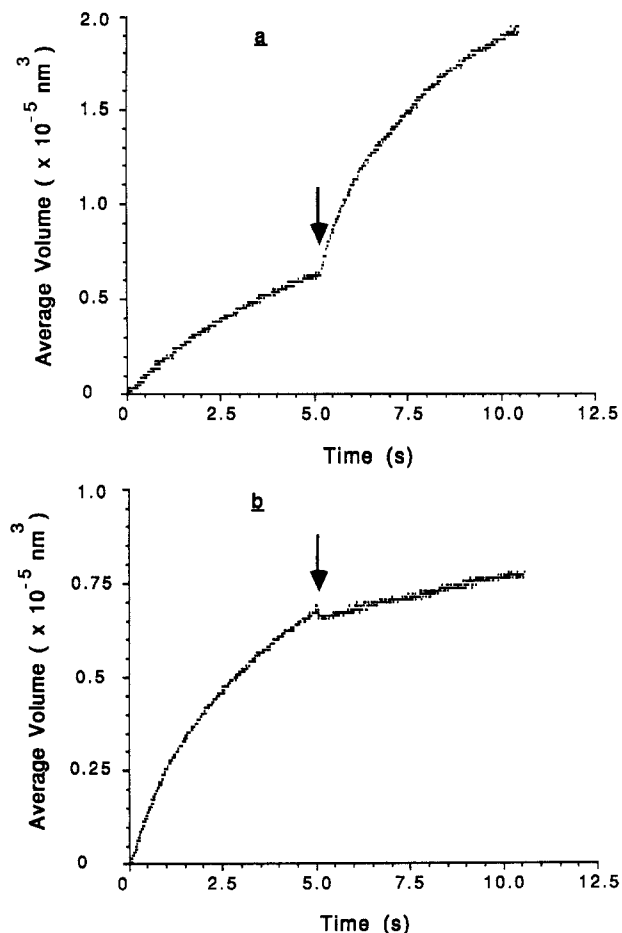


Figure 6. Average volumes of AgBr and AgI particles, measured 1 s after the pulse, as a function of  $[\text{X}^-]_0$ ;  $[\text{Ag}^+]_0 = 2.0 \times 10^{-4} \text{ M}$ . The volume of the particles for  $[\text{X}^-]_0 \geq 2.0 \times 10^{-4} \text{ M}$  was below the detection limit.

Light scattering measurements were performed for all three halides at several constant initial  $\text{Ag}^+$  concentrations and varying  $\text{X}^-$  concentration. Sizes obtained from these experiments, 1 s after the generation of bromide and iodide, are shown in Figure 6. Similar results were obtained for the chloride as well. For all halides and at all initial silver ion concentrations, the particle size abruptly drops below the detection limit when the initial halide ion concentration approaches or exceeds the initial concentration of  $\text{Ag}^+$ . This behavior is maintained for at least 20 s although the particles do grow on the time scale of minutes, even when the halide ion is in excess. On the very slow time scale, ripening is the major growth process, as observed previously.<sup>12b</sup>

The sharp decrease in growth rate is not due to formation of  $\text{AgX}_n^{(n-1)-}$  complexes since only for iodide is the formation of such complexes thermodynamically feasible. Furthermore, at the times where the light scattering intensity is still below our detection limit,



**Figure 7.** Double-pulse experiments to control size of AgI particles. Plotted are the average volumes of the particles as measured by light scattering. Arrows indicate the times of the second pulses. (a) Each pulse produces  $[I^-] = 2.1 \times 10^{-5}$  M. (b) Each pulse produces  $[I^-] = 1.1 \times 10^{-4}$  M. Solutions contain  $[Ag^+]_0 = 2.0 \times 10^{-4}$  M. Note the sharp decrease in growth rate following the second pulse in (b) as opposed to the increase in (a).

the spectral evolution indicates particles of appreciable sizes. Clearly the growth rate is asymmetric around the equivalence point and is strongly affected by the identity of the ion in excess. That this asymmetry does not result from early events, occurring at times prior to the observation by light scattering, is indicated by the double-pulse experiments illustrated in Figure 7. The first pulse in Figure 7b produces iodide ions at concentrations lower than the concentration of silver ions. The second pulse, however, increases the total iodide ion concentration beyond the equivalence point. As can be seen in Figure 7b, the growth rate is significantly reduced immediately after the second pulse. This behavior is in clear contrast to the results of Figure 7a, where the total iodide concentration following the second pulse remains below the equivalence point. In addition to reflecting on the mechanism of growth, the double-pulse experiments provide a method to control the size of the particles since the increase beyond the equivalence point could be induced at any time following the initial pulse.

The sharp decrease in growth rate is attributable to the effect of surface potential on the rate of agglomeration. In this time regime the concentration of particles far exceeds the concentration of the limiting ion in the solution. It is not surprising, therefore, that the growth is dominated by agglomeration of small particles. Under equilibrium conditions the surface potential of an AgI electrode is given by the Nernst equation:<sup>24</sup>

$$\psi = (kT/e) \ln ([Ag^+]/[Ag^+]_{iep}) \quad (14)$$

(24) Hiemenz, P. C. *Principles of Colloid and Surface Chemistry*; Marcel Dekker: New York, 1977.

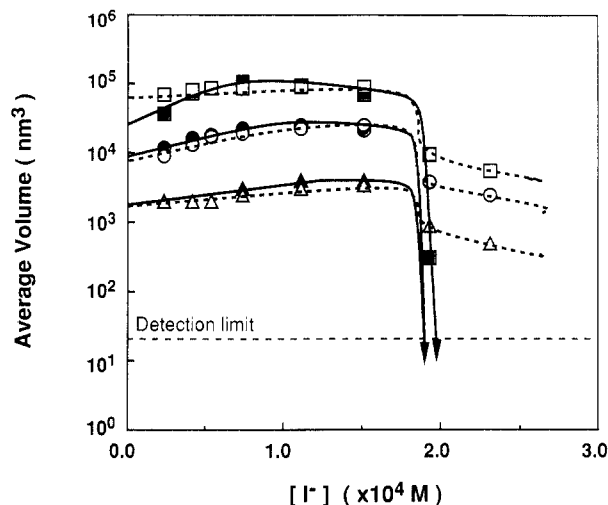


**Figure 8.** Effect of ionic strength on average volume of AgI aggregates in solution containing  $[Ag^+]_0 = 2 \times 10^{-4}$  M; no added salt (solid curves) and in the presence of  $5 \times 10^{-2}$  M NaClO<sub>4</sub> (dashed curves). Particle volumes measured at 0.1, 1.0, and 10 s for the lower, middle, and upper curves, respectively.

where  $[Ag^+]_{iep}$  represents the concentration of  $Ag^+$  at the isoelectric point (iep). The value of  $[Ag^+]$  for such a system in equilibrium with solid AgI can be determined from the solubility constant. In order for this equilibrium to be satisfied in a closed system  $[Ag^+]$  will be dramatically reduced when the iodide ion is produced in an amount equivalent to the initial  $[Ag^+]$ . This produces a correspondingly large increase in the magnitude of the surface potential.

The rate constant for aggregation of interacting colloidal particles was calculated in terms of the parameter  $W$ , defined by  $k = k_d/W$ , where  $k_d$  (assumed to be  $7.0 \times 10^9$  M<sup>-1</sup> s<sup>-1</sup>) is the diffusion-controlled rate constant in the absence of the interaction.  $W$  was estimated by numeric integration of eq 15,<sup>25</sup> where the

$$W = \int_{r_1+r_2}^{\infty} \frac{e^{\Phi/kt}}{R^2} dR \quad (15)$$

interaction energy,  $\Phi$ , was calculated using an approximate analytical solution to the DLVO theory.<sup>26,27</sup> The surface potential used to calculate  $\Phi$  was determined from eq 14. Changes in the magnitude of the surface potential of 20–40 mV, as occurs in the vicinity of the equivalence point, were sufficient to account for reductions in the aggregation rate constants by  $10^2$ – $10^3$ . However, in order to account for the continuous decrease in  $k$ , observed experimentally below the equivalence point (see below, e.g., Figure 9), a  $pAg_{iep} \leq 4.0$  had to be assumed. In contrast  $pAg_{iep} = 5.5$  has been measured for large particles.<sup>28</sup> However, the precise value for  $pAg_{iep}$  depends on experimental conditions; in particular the presence of alcohols (*tert*-butyl alcohol in our case) in solution reduces the value of  $pAg_{iep}$ .<sup>28b</sup> Furthermore, the Gibbs–Thomson effect<sup>29</sup> may alter the  $pAg_{iep}$  from that of bulk materials.

That the sharp drop in growth rate is electrostatic in origin was substantiated by the effect of ionic strength. Results in Figure 8 show the effect of adding  $5 \times 10^{-2}$  M NaClO<sub>4</sub> on the size of AgI particles at three different times. As can be seen in this figure, the added salt hardly affects the size of the particles when measured in excess  $Ag^+$ , in accordance with the assumption of a rather small negative surface potential in this concentration regime. However, as the equivalence point is approached, the size

(25) Fuchs, N. Z. *Phys.* **1934**, *89*, 736.

(26) Verwey, E. J. W.; Overbeek, J. Th. G. *Theory of the Stability of Lyophobic Colloids*; Elsevier: New York, 1948.

(27) Hogg, R.; Healy, T. W.; Fuerstenau, D. W. *Trans. Faraday Soc.* **1966**, *62*, 1638.

(28) (a) Ottewill, R. H.; Woodbridge, R. F. *J. Colloid Sci.* **1964**, *19*, 606. (b) Bijsterbosch, B. H.; Lyklema, J. *J. Colloid Sci.* **1965**, *20*, 665.

(29) (a) Mullin, J. W. *Crystallization*; 2nd ed.; CRC Press: Cleveland, 1972; Chapter 5, p 136. Walton, A. G. *The Formation and Properties of Precipitates*; Interscience: New York, 1967; Chapter 1, p 1.

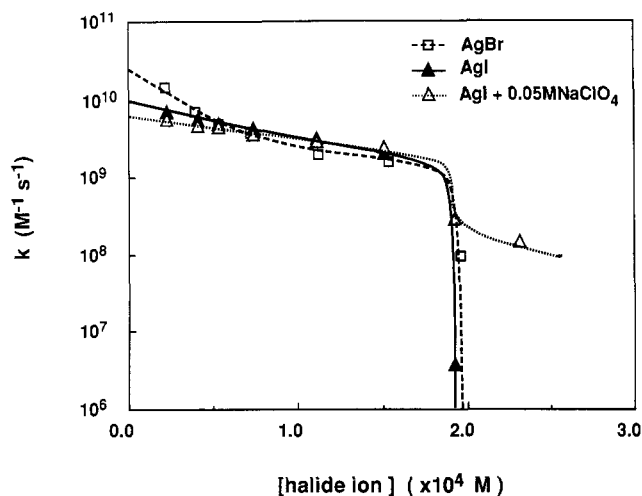


**Figure 9.** Rate constants for agglomeration of AgX at constant  $[Ag^+]_0 = 2.0 \times 10^{-4}$  M and varying  $[X^-]_0$  (i.e., the dose).

of the particles at any given time is much larger in the presence of the inert salt than in its absence. This indicates a substantially increased aggregation rate due to the screening of the electrostatic repulsion between the particles by the inert salt.

The kinetics of aggregation processes have been extensively discussed. As already shown by Kahlweit,<sup>30a</sup> the rate law for aggregation of particles of all sizes, in the absence of dissociation, can be expressed by eq 16, when all rate constants for agglom-

$$-dN/dt = kN^2 \quad (16)$$

eration of the various particles are equal. Applying the assumption of constant total particles volume,  $Nv = V$ , it is easy to see that  $dN = -(V/v^2) dv$ , which leads to

$$dv/dt = kNv \quad (17)$$

Thus a linear increase of the volume per particle with time is expected according to

$$v = kVt \quad (18)$$

It can be shown that this functional dependence of the particle volume on time is preserved for the volume-weighted average volume as well.<sup>30b</sup> Linear dependence of the volume on time was indeed observed for long periods of time for both AgBr and AgI, over the whole range of halide ion concentrations where rapid growth was observed (i.e., below the equivalence point). The underlying assumptions of an agglomeration process with diffusion-controlled rate constants, substantially independent of particle size at nearly constant, low surface potentials, seems to be correct. The rate constants calculated from linear plots according to eq 18 are shown in Figure 9. These rate constants are well within the range for diffusion-controlled processes between particles carrying small surface potentials. The rate constants slowly decrease upon increasing  $[X^-]_0$  nearly to the equivalence point, where they drop sharply. On the other hand, the average volume of a particle at a given time is nearly independent of  $[X^-]_0$ . This is particularly pronounced for the case of AgBr (e.g., Figure 6). Thus the decrease in  $k$  compensates for the increase in  $V$  leading to a nearly constant  $kV$  term in eq 18, and the particle volume is, by coincidence, nearly independent of initial halide ion concentration in this concentration regime (excess  $Ag^+$ ). The agglomeration mechanism may also provide a rationale for the broader size distribution indicated by the observed absorption spectra when the growth process is faster (i.e., at low iodide concentrations). Practically any agglomeration theory predicts that slower growth leads to more compact structures. At the slower rates, and therefore when the surface potentials are high, the more regular

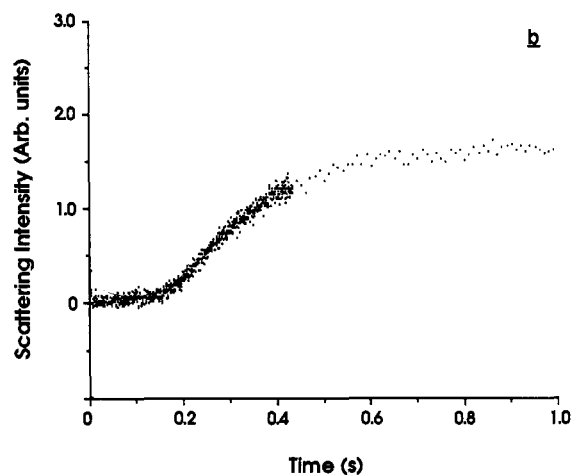
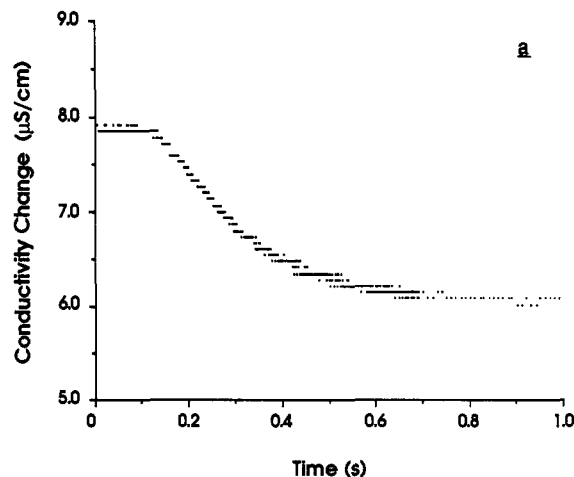


**Figure 10.** Induction periods in the growth of AgCl. (a) Disappearance of ions as measured by conductivity; (b) growth of particles as measured by light scattering.  $[Cl^-] = (1.6 \pm 0.1) \times 10^{-5}$  M for both (a) and (b).  $[Ag^+]_0 = 2.0 \times 10^{-4}$  M. Note that  $t = 0$  indicates the time of the pulse.

and compact packing of the growing particles is due to preferential adhesion of the approaching particles to areas of lower surface potential.<sup>31</sup>

**F. Growth of Nuclei.** The smaller stability constant of AgCl molecules (Table II) as compared to the other halides leads to a different growth mechanism at early times for this halide. Following the initial equilibration, reaction 11, an induction period ensues, during which no measurable drop in the conductance of the solution could be observed. At later times further reaction occurs and the conductivity drops to a final level, which is consistent with a quantitative reaction of all the  $Cl^-$  with  $Ag^+$  ions. A typical example of the induction period and the further decrease in conductivity is shown in Figure 10a. This result indicates that only a small fraction of the AgCl molecules is consumed during the induction period. Any major change in the equilibrium concentration of molecular AgCl, due to conversion to  $(AgCl)_n$  clusters, would produce a corresponding change in ion concentrations that would have been registered in the conductivity measurements.

An induction period is also observed before the light scattering signal starts to increase (Figure 10b). For the same initial ion concentrations the induction period is the same, within experimental accuracy, whether measured by conductivity or by light scattering. This correspondence of the induction periods is shown in Figure 11a. Taken together these results indicate that during the induction period particles of AgCl are formed that are large enough to serve as nucleation centers for further growth, yet during this same period of time very little molecular AgCl is consumed.

(30) (a) Kahlweit, M. In *Physical Chemistry, an Advanced Treatise*; Eyring, H., Ed.; Academic Press: New York, 1975; Vol. VII, p 675. (b) Ziff, R. M. In *Kinetics of Aggregation and Gelation*; Family, F., Landau, D. P., Eds.; Elsevier: Amsterdam, 1984; p 191.

(31) Thomas, I. L.; McCorkle, K. H. *J. Colloid Interface Sci.* **1971**, *36*, 110.

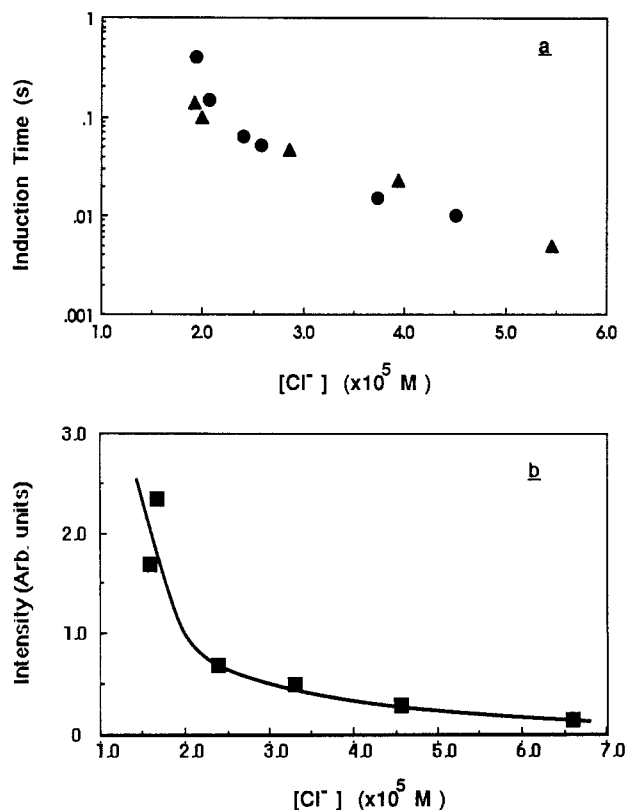


**Figure 11.** (a) Dependence of the induction period (circles from conductivity; triangles from light scattering) and (b) of the plateau level of light scattering intensity, on  $[\text{Cl}^-]_0$  during nucleation of AgCl.  $[\text{Ag}^+]_0 = 2.0 \times 10^{-4}$  M.

As the initial concentration of  $\text{Cl}^-$  produced by the irradiation is increased, the induction period shortens while the rate of the conductivity decay and the rate of increase in the light scattering both increase.

Induction periods during nucleation and growth processes have often been observed and extensively discussed in the literature.<sup>29,32</sup> Often the induction period,  $\tau$ , is empirically described by  $\tau = \alpha c^{-p}$ ,<sup>33</sup> where  $\alpha$  and  $p$  are constants and  $c$  is the ion concentration. The induction periods shown in Figure 11a are 2–4 orders of magnitude shorter than those reported previously by Kobayashi for AgCl<sup>34</sup> and a value of  $p = 3.4$  is presently obtained as compared to the earlier value of  $p = 5.0$ . However, the physical significance of these parameters is questionable.<sup>29b</sup> The underlying rationale for the appearance of induction periods is based on the Gibbs–Thomson equation which relates the solubility,  $S$ , of a particle to its radius:

$$r = \frac{2\gamma v_m}{RT \ln S} \quad (19)$$

Assuming bulk values for the interfacial tension,  $\gamma = 90 \text{ mJ/m}^2$ ,<sup>35</sup> and for  $v_m$ , the molar volume, one can calculate the critical radius,  $r_c$ , above which growth is thermodynamically favorable. For the chloride concentration range in which an induction period is observed ( $(1.0\text{--}6.0) \times 10^{-5}$  M),  $r_c = 9.3\text{--}5.3 \text{ \AA}$  is obtained. The corresponding aggregation number decreases from 80 to 15. The critical size thus decreases, and the concentration of aggregates of sizes larger than the critical size is expected to increase, as the chloride concentration increases.

Following the induction period the light scattering signal does not increase linearly with time (Figure 10b), as would be expected from an aggregation mechanism. The shape of the conductivity

and light scattering signals can quantitatively be explained by the addition of ions to a constant number of nuclei,  $N$ . Assuming a constant rate parameter,  $k$ , for the reaction of  $\text{Cl}^-$  with these nuclei, an exponential decay of  $[\text{Cl}^-]$  is expected, according to eq 20, and is experimentally observed (Figure 10a). Furthermore,

$$[\text{Cl}^-]_{\text{react}}/[\text{Cl}^-]_0 = 1 - e^{-kNt} \quad (20)$$

because the volume of the particle growing from the nucleus is proportional to  $[\text{Cl}^-]_{\text{react}}$ , and the light scattering signal is proportional to  $v^2$ , it should be of the functional form of  $(1 - e^{-kNt})^2$ . The S-shape dependence of the light intensity predicted by this functional form is indeed observed in Figure 10b.

As can be seen in Figure 10b, the scattered light signal reaches a plateau level at the end of the process of nuclei growth. It should, however, be emphasized that this apparent plateau is only a transition to a region of slower growth rate. In fact, the particles do continue to grow, and the growth by agglomeration process, described in section E, becomes the dominant growth mechanism. At the plateau level all of the AgCl material has been converted to particles that contribute to the light scattering signal (i.e., the situation described by eq I and III of the Experimental Section has been achieved). The light scattering signal is then given by

$$I_\infty = (1/N)\alpha v_m^2 [\text{Cl}^-]_0^2 \quad (21)$$

Experimentally, a decrease in  $I_\infty$  and an increase in  $kN$  is observed upon increasing  $[\text{Cl}^-]_0$  (Figure 11b). For  $I_\infty$  to decrease with increasing  $[\text{Cl}^-]_0$ , it has to be proportional to  $[\text{Cl}^-]_0^j$ , where  $j > 2$ . The results in Figure 11b yield  $j = 3$ , which leads to  $N \propto [\text{Cl}^-]_0^{-3}$  over the limited range of concentrations studied.

**G. Growth and Absorption Spectra.** Some information on growth processes at the early stages, when the sizes are below the detection limit of light scattering, can be extracted from spectroscopic measurements similar to those shown in Figures 3 and 5. As previously shown,<sup>12b</sup> size estimates from the absorption spectra of AgI using the “particle in the box” model are in good agreement with those obtained from light scattering. The radii calculated from the position of the peak of the exciton band seen in the spectra at early times (50  $\mu\text{s}$  to 1 ms) are shown in Figure 12, for the two  $[\text{I}^-]/[\text{Ag}^+]$  ratios of Figure 3a,b. At very early times the sizes for the excess initial  $\text{I}^-$  concentration are larger than for those in excess  $\text{Ag}^+$ . This is to be expected from an aggregation mechanism if the rate constants are similar in both solutions, since a higher total concentration of AgI is present in the former. At ca. 200  $\mu\text{s}$ , however, the exciton energies are the same for both concentrations, and at later times the particles at lower AgI concentrations are larger than at the higher concentration. This was attributed (section E) to the higher negative surface potential in solutions of excess initial iodide concentrations. Accordingly, the crossover point in Figure 12 indicates that at this time the surface potential has already developed to high enough values as to compensate for the higher total particle concentration. This is approximately the time required for the oscillator strength to attain a constant value for the higher AgI concentration. Assuming that once the oscillator strength is constant, bulk values of the various parameters (crystal parameters, density, effective masses) can be assigned to the growing particles, one concludes that the evolution of the surface potential follows concomitantly with the evolution of bulk properties.

Attempts were made to synthesize the evolution of the exciton band absorption for both concentration ratios of Figures 3 and 5. The fraction of the total AgI material that exists as particles of aggregation number  $i$  at time  $t$ ,  $N_{i,t}/N_{1,0}$ , was calculated from the kinetic model for aggregation, using eq 22, for all sizes up

$$\frac{N_i}{N_{1,0}} = (kN_{1,0}t)^{i-1} (1 + kN_{1,0}t)^{-(i+1)} \quad (22)$$

to  $i = 10^4$ ,<sup>30</sup> where  $N_{1,0} = [\text{AgI}]$ , i.e., the total AgI material. For each fraction the volume,  $v_i = iv_m$ , was then calculated and the energy of its exciton band is in turn calculated from the “particle in the box” model.<sup>1,2</sup> Each of these exciton bands was assumed to be Lorentzian and was assigned a half-height bandwidth of  $\Delta v$

(32) Söhnel, O.; Mullin, J. W. *J. Colloid Interface Sci.* **1988**, *123*, 43.

(33) (a) Christiansen, J. A.; Nielsen, A. E. *Acta Chem. Scand.* **1951**, *5*, 673, 675. (b) Nielsen, A. E. *J. Colloid Sci.* **1955**, *10*, 576.

(34) Kobayashi, K. *Sci. Rep. Tohoku Imp. Univ., Ser. 1* **1953**, *37*, 125, as quoted in ref 33b.

(35) Nielsen, A. E.; Söhnel, O. *J. Cryst. Growth* **1971**, *11*, 233.

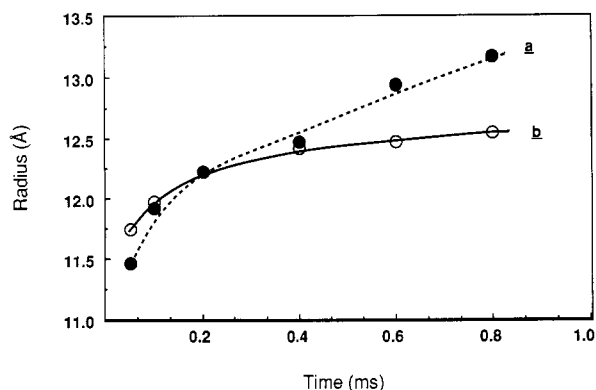


**Figure 12.** Radii of growing AgI clusters at early times calculated from the spectra of Figure 3 and 5, using the particle in the box model; a and b correspond to the experimental conditions given in Figure 3.

(arbitrarily assumed to be 0.1 eV), and the full band shape was then calculated. The intensity of absorption at any wavelength is obtained by summation of the contributions to the intensity from all  $i$  sizes assuming that the intensity is proportional to  $iN_i g(\nu)$ , where  $g(\nu)$  is the Lorentzian shape function. Results of these calculations are shown in Figure 13a for the spectra of the lower AgI concentration of Figures 3a and 5a. Since the model is expected to fail for very small sizes, particles of less than 40 molecules per particle were not included in the calculated absorption spectra. No absorption other than the lowest exciton region was included in the calculation, and thus the overall shapes of the calculated spectra at shorter wavelengths are not expected to mimic those experimentally observed. The calculations do, however, agree with the experimental observations in two features. The position of the exciton peak is reasonably well described by the modeling and the increase in the absorption intensity, experimentally observed at low [AgI] (Figures 3a and 5a), is also predicted.

An aggregation model with a constant rate parameter could not predict the absorption spectra recorded in high-dose experiments (Figure 5b). To model the spectral evolution under these conditions, a normal distribution of volumes, with a constant standard deviation of 10%, maintained during the growth process was assumed. Figure 13b presents the predicted spectra calculated in this manner. Such spectra retain an almost constant shape and intensity. Thus the different spectral evolution and the slower growth rate for the higher doses require a change in the growth mechanism. A ripening mechanism is compatible with the evolution of a normal size distribution. Apparently the decrease in rate of aggregation, imposed by the surface potential, is sufficient to allow a ripening mechanism to dominate.

### Conclusions

The utility of the pulse radiolysis technique to instantaneously produce a homogeneous, supersaturated solution of the component ions of a sparingly soluble salt has been demonstrated. While in this study we focus on silver halides, the technique is quite general in its ability to release other anions from the corresponding organic parent compound. Generation of sulfide by the same technique has been recently demonstrated.<sup>36</sup> Overall, the combination of several detection techniques with the superior time resolution of the pulse radiolytic initiation of growth has provided detailed experimental information on both the growth process and the effect of size on electronic properties for the silver halide species. The initial reaction between  $\text{Ag}^+$  and halide ions, as determined by conductivity measurements, proceeds at a diffusion-controlled rate,

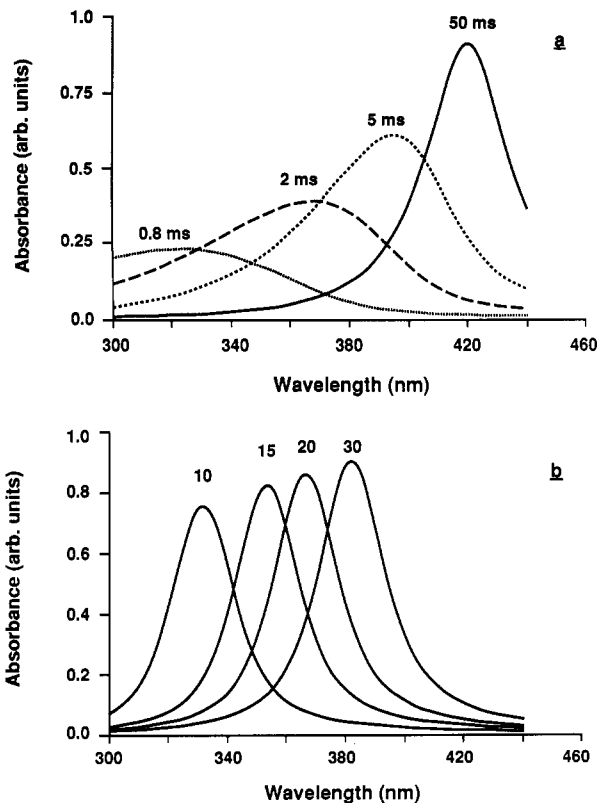


**Figure 13.** Calculated lowest energy exciton band of AgI using particle in the box model and assuming Lorentzian line shape of  $\Delta\nu = 0.1$  eV. (a) Particle size distribution as a function of time was calculated using eq 22; [AgI] =  $2.5 \times 10^{-5}$  M;  $k_d = 5.0 \times 10^9$  M<sup>-1</sup> s<sup>-1</sup>. (b) Normal particle size distribution assumed about the mean volume shown in the figure (in nm<sup>3</sup>) with a standard deviation of 10% of the mean.

rapidly establishing an equilibrium between AgX molecules and the ions. The rate of dissociation of the different silver halide molecules, however, varies substantially.

Subsequent growth of nuclei may then be viewed as a competition between aggregation and growth by successive addition of ions. When the salt is very insoluble, aggregation will dominate, provided its rate is not substantially reduced either by surface potential effects or by the decrease in particles concentration with growth. For the very insoluble AgI and AgBr species our results indicate that their growth can be described as an aggregation mechanism from very early times. When the salt is more soluble, the equilibrium concentration of ions may be large enough and the concentration of critical size particles small enough (e.g., the AgCl case) to allow early growth primarily by addition of ions to the nuclei. Furthermore, the size of the critical nucleus, determined by the increased solubility of particles of reduced radii as described by the Gibbs–Thomson equation, is larger for this case as compared to the previous one.

For AgI spectroscopic measurements have also been undertaken. The evolution of the optical absorption of AgI from the molecular species all the way to particles of bulk band gap was recorded. The shift in position of the band gap due to the confinement of the electron–hole pair in reduced dimensions is easily observed in the evolving spectra. The differences in growth rate due to electrostatic effects were also apparent in the spectra of the growing particles. Spectra obtained after  $\approx 100$   $\mu$ s of growth indicate that the initial growth process is rapid for all cases and that the surface potential develops during this time regime.

**Acknowledgment.** We thank D. Ficht and G. Cox for dedicated operation of the linac and G. Mills and L. Zongguan for electron microscopy results. Work performed under the auspices of the Office of Basic Energy Sciences, Division of Chemical Science, US-DOE, under Contract No. W-31-109-ENG-38.

**Registry No.**  $\text{CH}_2\text{Br}_2$ , 74-95-3;  $\text{CH}_2\text{I}_2$ , 75-11-6;  $^1\text{H}$ , 12385-13-6; AgI, 7783-96-2; AgBr, 7785-23-1; AgCl, 7783-90-6.

(36) Hayes, D.; Mičić, O. I.; Nenadović, M. T.; Swayambunathan, V.; Meisel, D. *J. Phys. Chem.*, in press.

(37) Critical Review of Rate Constants for Reactions of Hydrated Electrons, Hydrogen Atoms and Hydroxyl Radicals in Aqueous Solution. Buxton, G. V., Greenstock, C. L., Helman, W. P., Ross, A. B., Eds. *J. Phys. Chem. Ref. Data* 1988, 17, 513.

(38) Martel, A. E.; Smith, R. M. *Critical Stability Constants*; Plenum Press: New York, London, 1982.